





Laboratory Studies of Brine Growth Kinetics Relevant to Deliquescence on Mars

Raina V. Gough¹ , Danielle L. Nuding², Germán M. Martínez³, Edgard G. Rivera-Valentín³ , Katherine M. Primm⁴, and Margaret A. Tolbert¹

¹ Cooperative Institute for Research in Environmental Sciences and Department of Chemistry, University of Colorado, Boulder, CO 80309, USA
raina.gough@colorado.edu

² Jet Propulsion Laboratory/California Institute of Technology, Pasadena, CA 91109, USA

³ Lunar and Planetary Institute, Universities Space Research Association, Houston, TX 77058, USA

⁴ Planetary Science Institute, 1700 East Fort Lowell, Suite 106, Tucson, AZ 85719, USA

Received 2022 July 1; revised 2023 February 13; accepted 2023 February 18; published 2023 March 15

Abstract

Although previous studies have shown that the near-surface environmental conditions on Mars may permit salt deliquescence and therefore brine production, there is significant uncertainty in the kinetics of the process. Indeed, experimental studies have shown that deliquescence is either very rapid or too slow to be relevant to Mars. To resolve this uncertainty, we performed laboratory experiments to investigate the growth rate of Mars-relevant calcium perchlorate brines over a range of temperatures (184–273 K) and water vapor pressures (0.2–220 Pa). We show that the brine growth is faster at higher water vapor pressures and lower temperatures and for smaller particles. From our data, we determined a temperature-dependent net uptake coefficient for gas phase water molecules colliding with a perchlorate brine surface in the range of 3.8×10^{-4} at 185 K to 4.2×10^{-6} at 273 K. These values suggest that deliquescence on Mars is likely to be slow even when conditions thermodynamically permit a brine to form. We find that along the Curiosity rover traverse at Gale Crater, the near-surface conditions would only allow particles $<1 \mu\text{m}$ to fully deliquesce over a typical sol. At the higher-latitude Phoenix landing site, deliquescence may be 30% faster due to the higher water vapor pressures, but still, only micron-scale salt grains or coatings would be expected to deliquesce during a typical sol. These results suggest that brines formed via deliquescence on the surface of Mars are likely only present on small scales that may not be readily detected using conductivity or imaging techniques.

Unified Astronomy Thesaurus concepts: Mars (1007); Water vapor (1791); Regolith (2294); Chemical kinetics (2233)

1. Introduction

Since the discovery of perchlorate and other oxychlorine salts on Mars over a decade ago (Hecht et al. 2009), many studies have examined the brine-forming properties of these salts. Perchlorates, for example, can significantly depress the freezing point of water due to their low eutectic temperatures (Pestova et al. 2005; Chevrier et al. 2009; Renno et al. 2009; Zorzano et al. 2009). These salts can also deliquesce, meaning they can absorb water vapor and transition to an aqueous solution if the temperature is above the salt's eutectic temperature (T_E) and the relative humidity is above the salt's deliquescence relative humidity (DRH) value (Zorzano et al. 2009; Gough et al. 2011; Nuding et al. 2014; Nikolakakos & Whiteway 2015; Primm et al. 2017; Peng et al. 2021). For many perchlorate salts, these DRH values can be quite low, although values typically increase as temperature decreases. Previous work has measured a DRH value of 35% for NaClO_4 (Gough et al. 2011), 55% for $\text{Mg}(\text{ClO}_4)_2$ (Gough et al. 2011), and 55% for $\text{Ca}(\text{ClO}_4)_2$ (Nuding et al. 2014), all measured at 223 K. Although these low DRH values and temperature combinations may occur on the surface of present-day Mars

(e.g., Martín-Torres et al. 2015; Rivera-Valentín et al. 2018, 2020), some uncertainties remain.

Uncertainty in the feasibility of salt deliquescence on present-day Mars is primarily due to (1) uncertainty in the kinetics of deliquescence (Gough et al. 2011; Fischer et al. 2014) and (2) the relevance of laboratory conditions to Mars (Rivera-Valentín et al. 2021). There is a significant source of variability in previous works in regard to kinetics. For example, Fischer et al. (2014) found that when water vapor was the only source of water (as opposed to salts also being in contact with ice), deliquescence of $\text{Ca}(\text{ClO}_4)_2$ was slow and did not occur to a measurable extent over the 3.5 hr duration of the study conducted at 100% relative humidity (RH) and a temperature of 223 K. Additionally, Wang et al. (2019) measured the time for complete deliquescence of oxychlorine species and also found that deliquescence of $\text{Ca}(\text{ClO}_4)_2$ was slow and highly dependent on temperature. At 232 K, Wang et al. (2019) estimated 172 sols for the complete deliquescence of $\text{Ca}(\text{ClO}_4)_2$. On the other hand, Zorzano et al. (2009) observed NaClO_4 deliquescing in the lab on the order of minutes. Nuding et al. (2014) also found that perchlorate brines could form quite rapidly and also that, once formed, the $\text{Ca}(\text{ClO}_4)_2$ brines could persist under Martian subsurface conditions over an entire sol. Furthermore, laboratory studies have examined samples with sizes ranging from individual $\sim 10 \mu\text{m}$ particles (Gough et al. 2011; Nuding et al. 2014; Primm et al. 2017) to multiple layers of $>100 \mu\text{m}$ particles (Fischer et al. 2014) or larger (Wang et al. 2019). Additionally, lab studies have largely been performed under environmental conditions that are

⁵ Now at Johns Hopkins University Applied Physics Laboratory, Laurel, MD 20723



somewhat warmer and wetter than most locations on the Martian surface or shallow subsurface (Rivera-Valentín et al. 2021). Both warmer temperatures and higher water vapor partial pressures may support deliquescence and subsequent brine growth. In contrast, surface temperature and relative humidity conditions on Mars are related such that high relative humidities only occur at low temperatures, and low relative humidities occur at high temperatures (Martínez et al. 2017; Fischer et al. 2019; Rivera-Valentín et al. 2020).

To date, many investigations have assumed that deliquescence is an instantaneous process once the temperature and relative humidity conditions become thermodynamically favorable (Chevrier et al. 2009; Gough et al. 2011; Martín-Torres et al. 2015; Pal & Kereszturi 2017; Rivera-Valentín et al. 2020, 2018; Pál & Kereszturi 2022). However, in order to definitively determine if such brines form and to what extent, not only must the thermodynamics be favorable but the kinetics as well. Here we experimentally investigate the growth rate of a deliquesced perchlorate salt, calcium perchlorate. Specifically, we study how temperature and water vapor pressure affect the brine growth rate by measuring a temperature-dependent net uptake coefficient for water molecules colliding with a perchlorate brine surface. We use these results to estimate potential brine growth rates at two locations on Mars, the equatorial Gale Crater and the northern midlatitude Phoenix landing site, and determine if brine formation via deliquescence is feasible.

The temperature range we study (184–273 K) is very similar to the Martian surface temperatures measured by recent missions: Phoenix (Fischer et al. 2019), Mars Science Laboratory (MSL; Martínez et al. 2016, 2021), and Mars 2020 (Tamppari et al. 2022). The water vapor pressure measured by these missions, especially during the overnight hours on which we will focus here, is typically an order of magnitude lower than the lowest water vapor pressure used in our experiments of 0.2 Pa. However, our large experimental range of water partial pressures, $P_{\text{H}_2\text{O}}$, of 0.2–220 Pa will allow trends to be observed.

We selected calcium perchlorate as our sample in this study for several reasons. First, it may be the most Mars-relevant oxychlorine salt, detected in the soils at both Gale Crater (Glavin et al. 2013) and the Phoenix landing site (Kounaves et al. 2014) at concentrations from approximately 0.1 to 0.5 wt% (Stern et al. 2017). Oxychlorine species in general are likely globally distributed due to their potential atmospheric formation mechanism (Catling et al. 2010). Also, calcium perchlorate has a low T_E of 198 or 199 K (Pestova et al. 2005; Marion et al. 2010), the lowest of the pure perchlorate salts likely present on Mars. Not only does this low T_E increase the chances of brine formation at the low surface temperatures of Mars, but the large temperature range over which calcium perchlorate brine can form provides a large temperature range over which to study the temperature dependence of brine growth kinetics. Additionally, this salt has the ability to undergo metastable deliquescence at even lower relative humidity values and/or lower temperatures than predicted by equilibrium thermodynamics alone (Nuding et al. 2014; Gough et al. 2020). Finally, this salt is well studied (Fischer et al. 2014, 2016; Nuding et al. 2014, 2017; Heinz et al. 2016; Rivera-Valentín et al. 2018; Gough et al. 2020). This allows us to build on what is known about the deliquescence ability of

the salt and focus on an aspect that is not well known: the growth rate of a deliquesced brine.

2. Materials and Methods

2.1. Sample Preparation

An aqueous solution of 1 wt% $\text{Ca}(\text{ClO}_4)_2$ was prepared from $\text{Ca}(\text{ClO}_4)_2 \cdot 4\text{H}_2\text{O}$ (>99% pure, Sigma Aldrich). The solution was nebulized onto a hydrophobic quartz disk. The size range of the salt particles produced on the surface of the quartz disk was typically 5–20 μm in diameter. After a sample was made, it was placed into the dry (<1% relative humidity) environmental chamber and held at room temperature until any liquid-phase water was removed. In all cases, we used Raman spectroscopy to spectrally confirm that only a crystalline hydrate phase was present. Because the initial tetrahydrate had experienced a dissolution/recrystallization cycle during sample preparation, the salt may not have returned to the tetrahydrate phase specifically. In fact, in some cases, the crystalline phase was spectrally confirmed to be anhydrous (no O–H stretch), although it was often a hydrate. (See Gough et al. 2019 for details on the Raman spectral characterization of salt phases.) The Raman spectrometer was not used in this work otherwise; all other data in this study were obtained with the optical microscope.

2.2. Environmental Chamber and Microscope

The microscope and environmental chamber used here to study water uptake by brines have been previously described in detail (Baustian et al. 2010; Gough et al. 2011). Briefly, a Linkam environmental chamber was outfitted with an automated temperature controller and a Buck Research CR-1A chilled-mirror hygrometer attached to the chamber outlet. The sample was placed onto an indium foil-coated silver block inside the environmental chamber. The silver block, and thus the sample, was cooled to a desired temperature with a combination of continuously flowing liquid nitrogen and resistive heating. A platinum resistance sensor within the silver block monitored the sample temperature to ± 0.1 K. The environmental chamber was mounted on a high-precision motorized microscope stage that sits within the Raman microscope.

To vary the humidity inside the chamber, two gas flows were mixed before entering the chamber: dry N_2 and humidified N_2 . In both cases, the N_2 gas was of ultrahigh purity. The humidified N_2 was created by flowing gas through a glass frit submerged in deionized water. The ratio of these two gas streams was adjusted in order to achieve the desired relative humidity. Two different approaches were taken throughout these experiments in order to vary the relative humidity. In some experiments, H_2O vapor was increased or decreased gradually while temperature was held constant. In other experiments, the relative humidity was increased or decreased by lowering or raising the sample temperature, respectively, in the presence of constant water vapor pressure. Constant water vapor pressure was achieved by keeping the flow of humidified air constant.

A pump pulling at 1.0 L min^{-1} was attached to the outlet of the hygrometer, ensuring a constant airflow through the chamber and hygrometer. Frost point measurements from the hygrometer and sample temperature measurements from the platinum resistance sensor inside the silver block allowed for

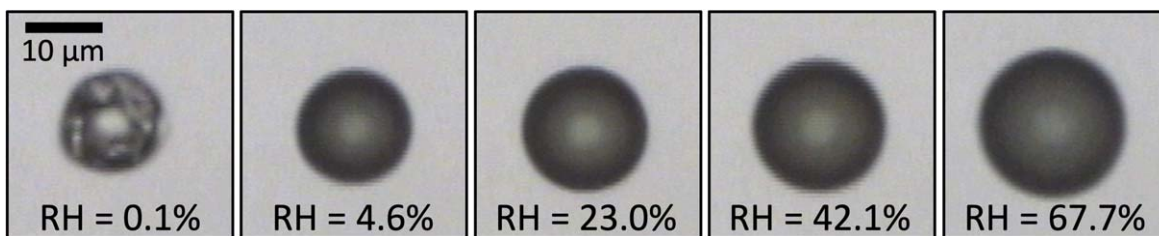


Figure 1. Microscope images of a single $\text{Ca}(\text{ClO}_4)_2$ particle collected at $50\times$ magnification. In this experiment, the relative humidity was increased, while the temperature of the salt sample was held constant at 273 K. The deliquescence phase transition from crystalline to aqueous occurred between 0.1% and 4.6% relative humidity. Then, for the remainder of the experiment, particle growth (water uptake) occurred.

real-time monitoring of the relative humidity at the sample. The uncertainty in relative humidity due to the uncertainty in the measured dew point was about $\pm 1.5\%$ relative humidity. The liquid N_2 lines were insulated and the chamber walls were at room temperature. This ensured that the sample was the coldest point within the chamber; thus, the relative humidity was always highest at the sample, minimizing adsorption of H_2O elsewhere.

During an experiment, the particles were monitored using the optical microscope (Olympus BX51). This microscope, typically used at $50\times$ magnification, was able to directly observe in real time any visual changes in the particles as they underwent deliquescence and subsequent growth. Images were collected regularly, typically at relative humidity increments of less than 5% relative humidity. This corresponded to time intervals typically between 3 and 15 minutes.

In this paper, all reported relative humidity values represent the relative humidity with respect to liquid at the temperature of the salt sample. As discussed in Rivera-Valentín et al. (2018), relative humidity sensors (RHSs) on Mars provide values with respect to ice following preflight calibrations of such sensors. This distinction is important because the difference between relative humidity with respect to ice versus liquid increases with decreasing temperature. The difference between these values can be as high as a factor of 2 at the low temperatures present at the Martian surface.

2.3. Particle Size Measurements

The diameters of the particles viewed by the optical microscope were measured using a custom LabVIEW particle sizing program. We began tracking particle growth immediately following the deliquescence phase transition. It was typically apparent when deliquescence began because the solid crystalline and aqueous liquid phases were visually distinct, as seen in Figure 1. Deliquescence occurred in this experiment between 0.1% and 4.6% relative humidity and resulted in a larger, darker, more homogeneous, and more spherical particle. This phase transition was rapid and almost always completed between the time two subsequent images were collected.

Particles were automatically identified with a shape detection function set to look for circular shapes. Figure 2 shows a representative microscope image with a typical field of view, which usually contained between two and four particles deemed large enough to monitor during the deliquescence/growth experiment. Very small particles and nonspherical particles were typically not identified. After the particles were identified, their diameters were measured assuming a circular shape. We excluded particles with a dry diameter below $5\ \mu\text{m}$ from our analysis in order to avoid the larger relative error associated with their size measurements. Particle area and

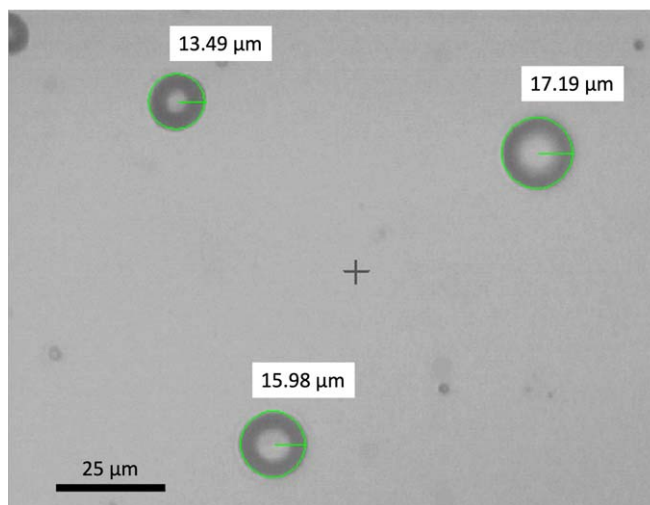


Figure 2. Typical microscope field of view showing $\text{Ca}(\text{ClO}_4)_2$ particles detected and measured by the LabVIEW particle sizing program. A few smaller particles were present, but they were smaller than our $5\ \mu\text{m}$ cutoff and not studied.

volume were calculated assuming half spheres. There is uncertainty associated with the assumption of circular shapes and also the assumption of half-spherical volume. The former is likely small, since we are working with liquid droplets that are generally spherical due to surface tension. The latter is difficult to quantify, since we have only a top-down view of the sample, and the 3D geometry of the particle is unknown.

2.4. Calculation of Growth Rate

After an experiment was completed, typically when the relative humidity was at or near 100%, the growth rate was calculated for each particle $>5\ \mu\text{m}$ in each collected image. For each time interval in minutes, t , between two consecutive images, image n and image $n + 1$, a normalized growth rate for that time period, Rate_{n+1} , in units of $\mu\text{m}^3\ \mu\text{m}^{-2}\ \text{minute}^{-1}$, was calculated as

$$\text{Rate}_{n+1} = \frac{V_{n+1} - V_n}{A_n t}, \quad (1)$$

where V_{n+1} and V_n are the volumes in μm^3 of a given particle in images $n + 1$ and n , respectively, and A_n is the surface area in μm^2 of the particle in image n . The growth rate was normalized to the particle surface area because the number of collisions between molecules of water vapor and the brine surface will be proportional to the available brine surface area.

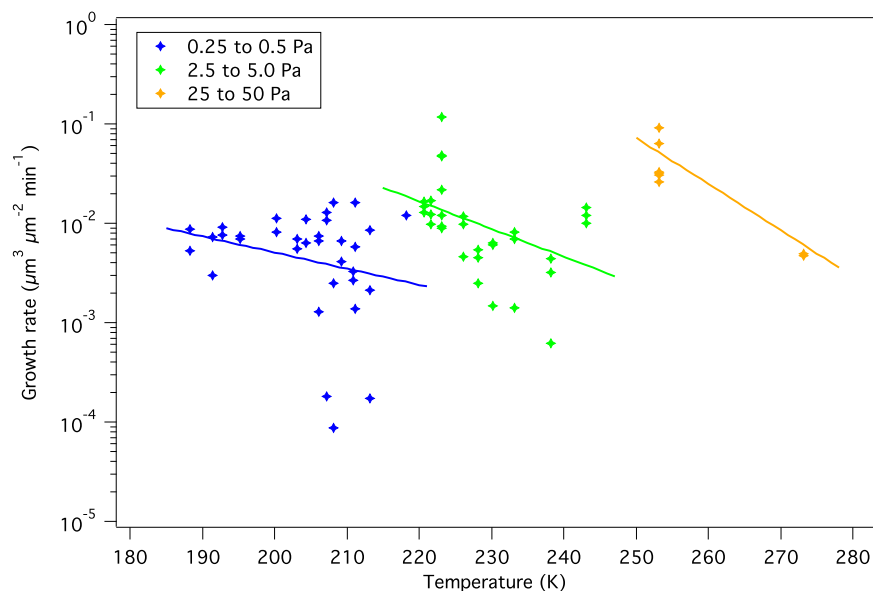


Figure 3. Normalized particle growth rate plotted as a function of temperature for three water vapor pressure bins spanning 3 orders of magnitude.

3. Results

3.1. Growth Rate as a Function of Temperature and Water Vapor Pressure

In total, 17 experiments were performed on $\text{Ca}(\text{ClO}_4)_2$ at a range of temperatures ($T = 184\text{--}273$ K) and water vapor pressures ($P_{\text{H}_2\text{O}} = 0.2\text{--}220$ Pa). A total of 38 particles were monitored during these experiments, with pre-deliquescence particle diameters ranging from 5.6 to 16.1 μm . Each experiment had, on average, seven images collected; thus, on average, six periods of growth were monitored. This resulted in approximately $38 \times 6 = 228$ calculated growth rate data points. Here we present these growth rates as a function of temperature and water vapor pressure. Often, both temperature and water vapor pressure varied throughout an experiment and therefore changed between images n and $n + 1$. Therefore, the temperature and water vapor pressure associated with a given growth rate data point represent the conditions present during the first of the two images (image n) used to obtain a given growth rate.

Figure 3 presents the normalized particle growth data as a function of sample temperature in kelvin. The data are binned by pressure, with this figure showing three water vapor pressure bins spanning three orders of magnitude: 0.25–0.5, 2.5–5.0, and 25–50 Pa. Only data in these three pressure bins were plotted; this was done to more clearly highlight the temperature- and pressure-dependency trends. An exponential fit is shown for each water vapor pressure bin. For data in the same water vapor pressure bin (same color data), it is clear that lower temperatures correspond to a higher growth rate of a brine droplet. This is as expected, since the uptake of water vapor by a surface should occur more easily at colder temperatures and thus lower collisional energies. This relationship was seen at all water vapor pressures studied. This temperature dependence was seen to slightly steepen at warmer temperatures. It can also be seen in Figure 3 that higher water vapor pressure leads to higher growth rates. This relationship between growth rate and water vapor pressure is also as expected. More water vapor should result in more collisions between water molecules and the salt surface and therefore a

higher likelihood of successful collisions that lead to water uptake and particle growth.

Figure 4 shows all particle growth rate data plotted in temperature versus water vapor pressure space. The color axis represents the normalized particle growth rate. The warmer-temperature experiments were performed at higher water vapor pressure values, and vice versa. This is because salt deliquescence is primarily dependent on relative humidity, and higher water vapor pressure is needed to achieve a given relative humidity at warmer temperatures. The specific temperature and water vapor pressure dependencies discussed in the previous paragraph are also visible in Figure 4. Growth rate increases with water vapor pressure at constant T (see, for example, the dotted rectangle at 273 K). The growth rate also increases with decreasing temperature at constant water vapor pressure (see, for example, the dashed rectangle centered at ~ 0.3 Pa). Additionally, when the ground temperature and water vapor pressures from the MSL Rover Environmental Monitoring Station (REMS; gray crosses) and Phoenix Thermal and Electrical Conductivity Probe (TECP; black plus signs) are plotted in the same phase space as the experimental data, we see that both span a similar temperature range. However, the lab experiments were performed at higher water vapor pressures than found on Mars. See Section 4.2 for more details on MSL and Phoenix instruments and data.

It should be noted that deliquescence was observed for each experiment plotted here, which includes temperatures down to 184 K. The eutectic temperature of $\text{Ca}(\text{ClO}_4)_2$ has been reported as between 198 and 199 K (Pestova et al. 2005; Marion et al. 2010); therefore, deliquescence was observed 15 K below this equilibrium eutectic temperature. This is not very surprising, as metastable processes involving this and other salts that allow a brine to form or persist below the stable eutectic temperature have been observed. Gough et al. (2020) reported water uptake by calcium perchlorate at temperatures as low as 183 K, and Primm et al. (2017) observed deliquescence of a chloride salt more than 20 K below its stable eutectic temperature. Furthermore, Toner et al. (2014) observed that many Mars-relevant perchlorate and chloride salts are able to supercool below the eutectic temperature, and the effect is

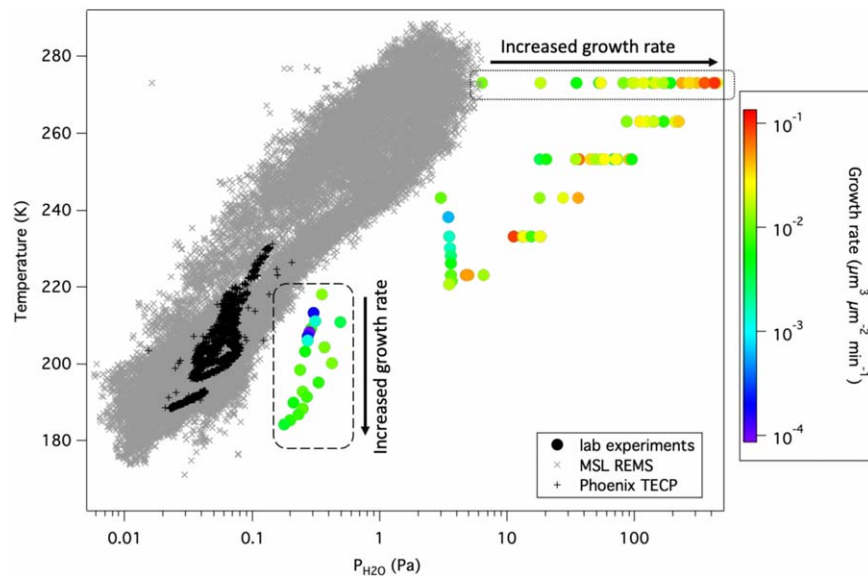


Figure 4. Normalized particle growth rate on color axis plotted in temperature vs. water vapor pressure space. It can be seen that the growth rate increases with water vapor pressure at constant T (see dotted rectangle) and increases with decreasing T at constant water vapor pressure (see dashed rectangle). Additionally, a comparison of our experimental data (colored circles) vs. the temperature and water vapor pressures measured by MSL REMS (gray crosses) and Phoenix TECP (black plus signs) shows that all span a similar temperature range, but the lab experiments were performed at higher water vapor pressure values.

especially large in the case of magnesium and calcium perchlorate.

3.2. Determination of the Net Uptake Coefficient, γ_{net}

The particle growth data were used to determine the value of the net uptake coefficient, γ_{net} , at each temperature. This term represents the fraction of collisions between water vapor molecules and the brine droplet surface that result in net uptake of water by the particle and loss from the gas phase. The approach we take is to compare the observed volume increase to the theoretical maximum volume increase to determine the fraction of successful collisions. The theoretical volume increase is what would occur if all collisions between water vapor molecules and the brine droplet resulted in uptake. This analysis was done for each time interval between consecutive microscope images. Note that the typical time interval between images, and thus the time period over which a typical γ_{net} value was determined, was between 3 and 15 minutes.

To calculate the theoretical maximum volume increase, the flux of water molecules, F_{H_2O} (molecules $m^{-2} s^{-1}$), to a particle surface during each time interval was calculated following

$$F_{H_2O} = \frac{1}{4} [H_2O] \omega, \quad (2)$$

where $[H_2O]$ is the water vapor concentration in the gas phase (molecules m^{-3}), and ω is the mean thermal velocity of the gas phase water molecules ($m s^{-1}$). The value of $[H_2O]$ was determined using the ideal gas law,

$$[H_2O] = \frac{P_{H_2O}}{R T}, \quad (3)$$

where P_{H_2O} is the partial pressure of water in pascal determined from the dew point temperature measured by the hygrometer at the outflow of the environmental chamber, R is the gas constant ($8.314 m^3 Pa K^{-1} mol^{-1}$), and T is the temperature of the gas

phase in kelvin. This gas phase temperature was not measured in our experiment but was assumed to be 273 K.

The value of ω , the mean thermal velocity, of the gas phase water molecules was determined following

$$\omega = \left(\frac{8RT}{\pi MM} \right)^{1/2}, \quad (4)$$

where MM represents the molar mass of H_2O , $0.018 kg mol^{-1}$. The gas phase temperature was again assumed to be 273 K, which resulted in a value of $567 m s^{-1}$ for ω in all cases.

Once the flux, F_{H_2O} , was determined, the theoretical volume increase of the particle if all collisions resulted in uptake of a water molecule, ΔV_{theor} , was determined from the product of the water vapor flux; the particle surface area, A ; and elapsed time, Δt , using

$$\Delta V_{theor} = F_{H_2O} \times A \times \Delta t. \quad (5)$$

As in previous calculations, the particle surface area was determined from the measured particle diameter assuming half-spherical volume. Finally, the net uptake coefficient, γ_{net} , was determined by dividing the actual volume increase observed in the time interval between two consecutive microscope images by the maximum theoretical volume increase over that same time period, ΔV_{max} (Equation (6)):

$$\gamma_{net} = \frac{V_{n+1} - V_n}{V_{max}}. \quad (6)$$

These γ_{net} values are plotted in Figure 5 as $\ln(\gamma_{net})$ versus inverse temperature. Every calculated γ_{net} point is represented by a small gray circle, and the average γ_{net} values are shown as large black circles. A linear fit through the data is shown in

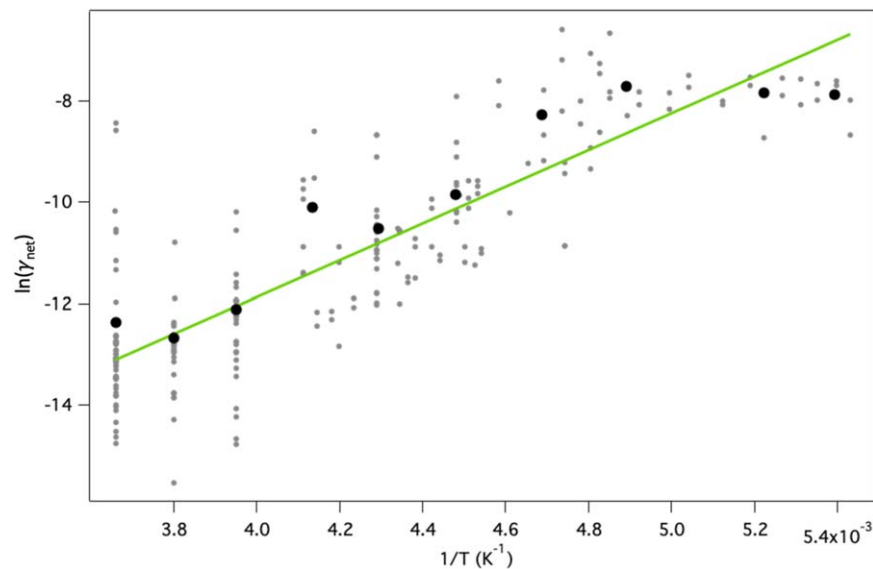


Figure 5. Values of the net uptake coefficient, γ_{net} , as a function of temperature, plotted here as $\ln(\gamma_{\text{net}})$ vs. $1/T$. Every individual γ_{net} value is shown as a small gray circle, and the large black circles represent the averaged γ_{net} values.

green and has the equation

$$\ln(\gamma_{\text{net}}) = 3628.2(1/T) - 26.385. \quad (7)$$

The values of γ_{net} that we calculate in this paper are net uptake coefficients that are based on our observations of particle growth. They consider the balance of molecules taken up by and lost from the surface over the time period between each pair of consecutive images. Previous work examining the uptake of water vapor onto surfaces such as water ice (Haynes et al. 1992), liquid water (Davidovits et al. 2004), or NaCl brine (Fung et al. 1987) determines the condensation and evaporation coefficients separately, as opposed to a net uptake coefficient value like we do here. Specifically, our ΔV_{max} (Equation (6)) assumes that all collisions result in uptake with no desorption occurring. As a result, the uptake or condensation values determined by the literature studies are much larger than ours (~ 3 orders of magnitude larger when temperature overlap enables comparison). A net value is suitable for estimating net growth, however. Below, we will use our γ_{net} values to apply the results of our experiments to the environment of the Martian surface to estimate likely brine growth rates.

4. Discussion

4.1. Pressure Correction of Experimentally Determined $\gamma_{\text{net}}(T)$

Before we applied our experimentally determined values of $\gamma_{\text{net}}(T)$ to Mars, the role of pressure dependence was considered. The laboratory experiments were performed under ambient atmospheric pressure conditions (8.39×10^4 Pa), and water molecules had to diffuse through these atmospheric gas molecules to reach the sample surface and collide with the salt. This may have impacted the value of our experimentally determined γ_{net} , with the “high” pressures present during the experiment lowering the value from what could be considered the “true” value at much lower pressures and longer mean free paths.

A pressure correction was performed as outlined in Tang et al. (2015). Our experimentally determined γ_{net} was treated as the effective uptake coefficient, γ_{eff} , in the Tang et al. correction analysis. Then, γ was determined using the process outlined in Equations (2), (3a), and (4)–(9) of Tang et al. The typical value of the gas transport coefficient, Γ_{diff} , was found to be on the order of 1×10^{-4} . It is likely that our small particle sizes and uptake coefficients resulted in limited impacts of gas phase diffusion, consistent with Tang et al. (2015). This Γ_{diff} value resulted in a difference of $<1\%$ between γ_{eff} and γ . Because the pressure dependence of gamma appears to be minor under our experimental conditions, no formal pressure correction was performed before applying our experimentally determined γ_{net} values to the lower-pressure environment of Mars.

4.2. Application of Results to Mars: Gale Crater and Phoenix Landing Site

Given the flux of atmospheric H_2O vapor molecules to salt surfaces in the Martian environment and the experimentally determined or extrapolated $\gamma_{\text{net}}(T)$ values, the time needed for a salt particle to fully deliquesce can be determined. Here we estimate this deliquescence time at both Gale Crater (home of the Curiosity rover) and the Phoenix landing site. These will be approximations, with the purpose of understanding the extent of possible brine formation at these locations.

Only limited extrapolation of our experimentally determined $\gamma_{\text{net}}(T)$ values was needed; however, there is an additional factor that must be considered when applying our results to Mars. Our experiments only investigated post-deliquescence particle growth, or the growth of a saturated brine droplet into a larger brine droplet (see the orange rectangle in the top panel of Figure 6). On Mars, only the initial stages of the deliquescence process are likely to occur. A solid salt grain may acquire a thin layer of saturated brine. This may then transition to a thicker layer of saturated brine or perhaps an entirely aqueous droplet (blue rectangle in the bottom panel of Figure 6). The difference between the laboratory system and a putative Martian system is due to the available water vapor, which is very abundant in our

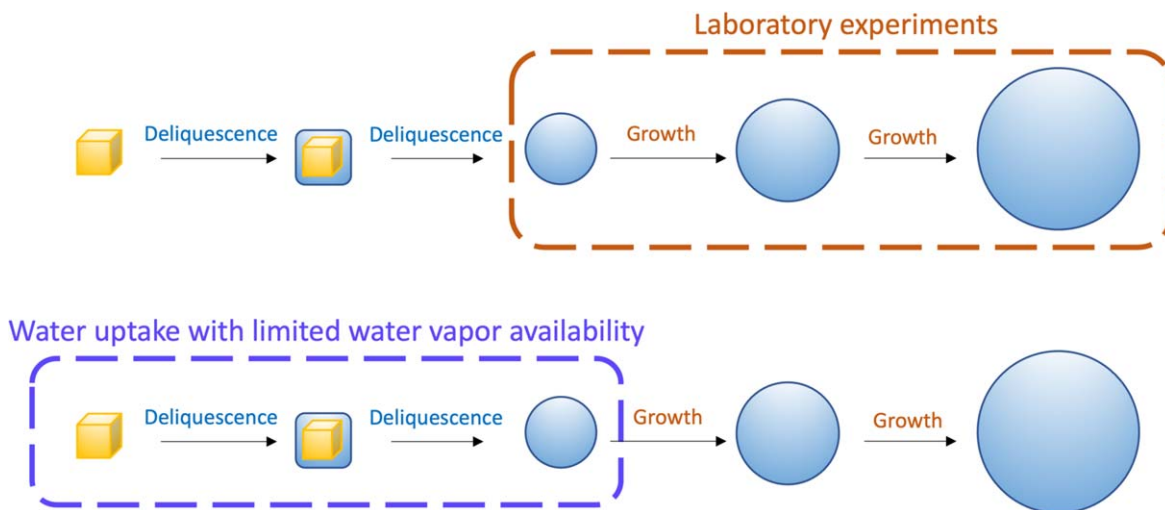


Figure 6. Schematic illustrating the difference between deliquescence and subsequent growth as it occurs in our laboratory experiments (orange rectangle) and may occur on Mars due to lower water vapor availability (blue rectangle). In both cases, however, the experimentally determined value of the net uptake coefficient for water molecules onto a brine surface is likely relevant.

lab experiments (the process is salt-limited) and very scarce on Mars (the process is water-limited). On Mars, though, the deliquescence process would still require water molecules to be taken up by a brine surface; thus, we theorize that our $\gamma_{\text{net}}(T)$ values (the net uptake of water vapor molecules onto a brine surface) are still relevant to deliquescence on Mars. It is possible that the initial stage of deliquescence, the first transition of crystalline salt into a saturated brine, is even slower than the subsequent brine growth. Although we were not able to study the kinetics of this initial deliquescence phase transition, our estimates of brine growth below may be upper limits.

4.2.1. Gale Crater

For the analysis at Gale Crater, we use three values measured by the REMS instrument suite on board the Curiosity rover (Harri et al. 2014): (1) ground temperature (T_g) measured by the ground temperature sensor (GTS; Sebastián et al. 2010), (2) the board temperature (T_b) of the RHS used to calibrate the sensor, and (3) the relative humidity with respect to ice at 1.6 m ($\text{RH}_{1.6\text{m}}$), also measured by the RHS. This $\text{RH}_{1.6\text{m}}$ value was used to calculate the water vapor partial pressure at 1.6 m ($P_{\text{H}_2\text{O},1.6\text{m}}$) using the saturation vapor pressure over ice at the corresponding measured T_b , as described in Appendix A of Martínez et al. (2016). All REMS measurements included here were collected during the first 4 s after the RHS had been turned on after it had been inactive for at least 5 minutes (Martínez et al. 2016). This was done to minimize the warming issues known to occur in the instrument. For more details about the data processing and filtering of GTS and RHS data, see Rivera-Valentín et al. (2018) and Martínez et al. (2021). Here we use data measured over the first 2500 sols of the mission.

In general, our experiments were performed under warmer and wetter conditions than found at the surface of Gale Crater, although there is some overlap in environmental conditions. The range of $P_{\text{H}_2\text{O},1.6\text{m}}$ values measured by REMS over the first 2500 sols is 0.006–6.2 Pa. The range of water pressures used in our experiments is 0.2–220 Pa. Each covers a range of about 3 orders of magnitude, with overlap between 0.2 and 6.2 Pa. The range of T_g values measured by the REMS GTS over the first

2500 sols is 171–255 K. The range of temperatures used in our experiments is 184–273 K, so there is overlap between 184 and 255 K. As was seen in Figure 4, however, there was no direct overlap between our experiments and Martian conditions when plotted in temperature versus water vapor pressure phase space. Our experiments typically contained an order of magnitude or two more water vapor at a given temperature. For an analysis of the environmental conditions at Gale Crater for the first 2500 sols of the MSL mission, the reader is referred to Martínez et al. (2021).

We focused on the late evening and early morning hours at Gale Crater for our analysis because these are the only times of day during which deliquescence may occur according to thermodynamics. For deliquescence to begin, the relative humidity must be higher than the DRH of a given salt, and the relative humidity is always higher overnight due to the lower ground and air temperatures. For the $\text{Ca}(\text{ClO}_4)_2$ salt studied here, the DRH values range from 10% at 273 K to 55% at 223 K (Nuding et al. 2014). At Gale Crater, the average relative humidity with respect to liquid at the planetary surface is $\geq 10\%$ only between the hours of 23:00 and 07:00 local time; therefore, this time period was selected for our deliquescence analysis. It should be noted that during this time of day, the temperature is likely to be below the T_E for this salt, so stable deliquescence may not occur even though the relative humidity criterion is met (Rivera-Valentín et al. 2018). As stated previously, though, metastable brines may form and exist below the T_E due to supercooling (Toner et al. 2014; Primm et al. 2017; Gough et al. 2020). During these overnight hours at Gale Crater, the average water vapor partial pressure at 1.6 m ($P_{\text{H}_2\text{O},1.6\text{m}}$) is 0.0425 Pa (range = 0.0064–0.0852 Pa), the average ground temperature (T_g) is 198 K (range 171.2–212.1 K), and the average air temperature at 1.6 m ($T_{1.6\text{m}}$) is 205.2 K (range = 183.1–229.6 K).

In order for a $\text{Ca}(\text{ClO}_4)_2$ particle to completely deliquesce, the salt grain must absorb sufficient water to form a saturated brine. For $\text{Ca}(\text{ClO}_4)_2$ at the T_E of 198 K, the water concentration in a eutectic brine is 50 wt% (Nuding et al. 2014). A brine containing a 50/50 mixture of $\text{Ca}(\text{ClO}_4)_2$ and water must contain 13.26 water molecules for every $\text{Ca}(\text{ClO}_4)_2$ formula unit based on the respective molar masses of anhydrous

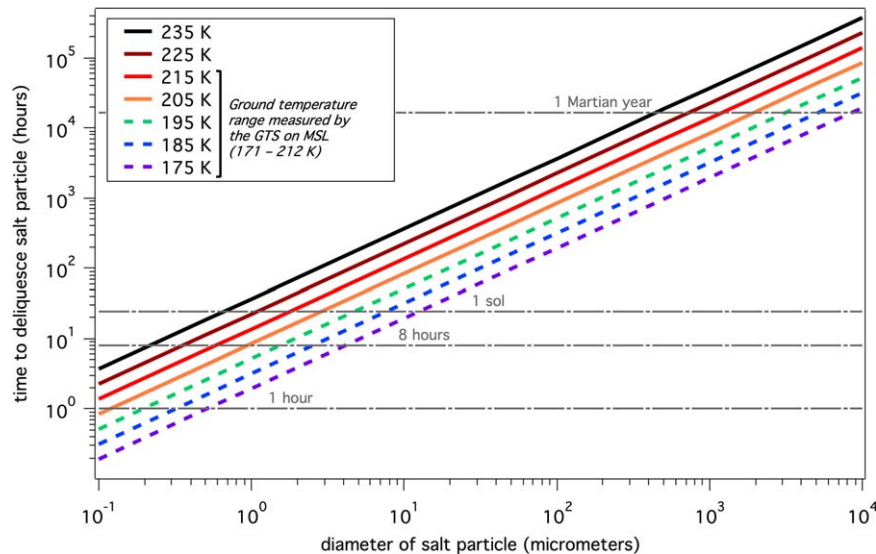


Figure 7. Time needed to fully deliquesce a $\text{Ca}(\text{ClO}_4)_2 \cdot 4\text{H}_2\text{O}$ grain at Gale Crater, Mars, as a function of the salt particle diameter in microns and the temperature of the salt particle. Solid colored lines are above the eutectic temperature of $\text{Ca}(\text{ClO}_4)_2$, and dashed colored lines are below the eutectic temperature (only metastable deliquescence possible). If only temperatures above the eutectic temperature of $\text{Ca}(\text{ClO}_4)_2$ (197 K) are considered, then only particles $< 1 \mu\text{m}$ will be able to fully deliquesce in less than 8 hr, which is the overnight duration of the conditions potentially favorable for deliquescence.

$\text{Ca}(\text{ClO}_4)_2$ ($238.97 \text{ g mol}^{-1}$) and water (18.02 g mol^{-1}). We assume the salt starts out as the tetrahydrate, $\text{Ca}(\text{ClO}_4)_2 \cdot 4\text{H}_2\text{O}$; so, to form the eutectic brine, all additional water molecules beyond the four waters of hydration ($13.26 - 4 = 9.26$ waters) must be acquired from the near-surface atmosphere. We determine the number of water molecules needed for a specific size spherical salt grain to deliquesce by converting the particle volume to mass with the $\text{Ca}(\text{ClO}_4)_2 \cdot 4\text{H}_2\text{O}$ density (2.65 g cm^{-3}) and then to moles of salt with the molar mass of $\text{Ca}(\text{ClO}_4)_2 \cdot 4\text{H}_2\text{O}$. Finally, each formula unit of $\text{Ca}(\text{ClO}_4)_2 \cdot 4\text{H}_2\text{O}$ requires an additional 9.26 water molecules to be absorbed in order for deliquescence to be complete.

We approximate the time, t , needed for this amount of water to be taken up by a spherical salt grain with surface area A assuming the flux ($F_{\text{H}_2\text{O}}$) given in Equation (2) and incorporating values of the experimentally determined uptake coefficient, $\gamma_{\text{net}}(T)$, as follows:

$$t = \frac{\text{water molecules needed to deliquesce}}{\gamma_{\text{net}}(T) F_{\text{H}_2\text{O}} A}, \quad (8)$$

where $F_{\text{H}_2\text{O}}$ was calculated using Equations (2)–(4) above. In Equation (3), a $P_{\text{H}_2\text{O},1.6\text{m}}$ value of 0.0425 Pa was used as $P_{\text{H}_2\text{O}}$, as this was the average $P_{\text{H}_2\text{O},1.6\text{m}}$ value measured by the REMS RHS between 23:00 and 07:00 local time. In Equations (3) and (4), the average T_b value of 205.2 K from the REMS RHS was used as T , as this was the average T_b value measured by the REMS RHS between 23:00 and 07:00 local time.

Finally, the range of REMS GTS T_g values during our time period of interest (23:00 and 07:00 local time) was 171.2 – 229.6 K . We chose, therefore, to examine the temperature range 175 – 235 K . These corresponding $\gamma_{\text{net}}(T_g)$ values were determined using Equation (7). We then used Equation (8) to determine the time required for complete deliquescence of a $\text{Ca}(\text{ClO}_4)_2 \cdot 4\text{H}_2\text{O}$ particle at Gale Crater assuming the average near-surface atmospheric conditions present between 23:00 and 07:00. These deliquescence time

values are shown in Figure 7 as a function of particle size and ground temperature.

As seen in Figure 7, larger particles and warmer temperatures result in longer deliquescence timescales. The latter is due to the temperature dependence of $\gamma_{\text{net}}(T)$. Horizontal gray lines in Figure 7 denote different time periods ranging from 1 hr to 1 Martian yr. Conditions even possibly conducive to deliquescence (average relative humidity $>$ DRH) will only last a maximum of 8 hr sol^{-1} at Gale Crater (23:00–07:00). During this time window, only particles with diameters $< 4 \mu\text{m}$ would be able to fully deliquesce given the temperature range found from 23:00 to 07:00 local time. If only temperatures above the T_E of $\text{Ca}(\text{ClO}_4)_2$ (198 or 199 K) are considered, then only particles $< 1 \mu\text{m}$ will be able to deliquesce overnight. Although this plot shows complete deliquescence of a given particle size, if deliquescence does occur, then all grain sizes will at least partially deliquesce to this thickness.

To date, there is no evidence of salt deliquescence at Gale Crater along the Curiosity traverse. Although oxychlorine salts like perchlorate were detected in many regolith and drilled rock samples at Gale Crater (Clark et al. 2021), the conditions at the surface are generally not conducive to brines due to the combination of subeutectic temperatures and dry (low water vapor pressure) conditions (Chevrier et al. 2020). Rivera-Valentín et al. (2018) reported, though, that deliquescence can potentially occur in the subsurface along the Curiosity rover traverse, particularly for terrains with low thermal inertia and high albedo (Martinez et al. 2021) during very specific times of year ($L_s = 100$ – 110). Here we add to this understanding by showing that if the conditions for deliquescence are met in the shallow subsurface of Gale Crater, the amount of brine formed will likely be very small, with only micron-scale salt grains or salt coatings able to deliquesce. These amounts of brine might be too small to detect visually by imaging cameras, even the Mars Hand Lens Imager, which, at its minimum working distance, is able to achieve a resolution of $\sim 14 \mu\text{m pixel}^{-1}$. The expected amount of water is also too little to be detected by the Sample Analysis at Mars—Evolved Gas Analyzer (SAM-EGA) and, in addition, would likely be lost in the ambient

environment of SAM (40°C) before the heating and evolved gas detection experiment began.

4.2.2. Phoenix Landing Site

At the Phoenix landing site, the measured conditions would more readily permit deliquescence of calcium perchlorate (Rivera-Valentín et al. 2020). Here, to determine deliquescence timescales at the Phoenix landing site, we used a similar approach as described in the above section about MSL at Gale Crater (Section 4.2.1.). Slightly different spacecraft instrument data were available, as we briefly describe here. We used near-surface environmental conditions measured by the TECP obtained from the latest recalibration described in Fischer et al. (2019), as well as by the Meteorological Station (MET) instrument (Taylor et al. 2008).

The TECP instrument contained an RHS and a temperature sensor on the electronics board. This probe also had four needles that could be inserted into the soil to measure the temperature, among other soil properties. When the 15 mm long needles were inserted into the soil, the humidity sensor was a few centimeters above the ground. Like with MSL, the measured relative humidity and the board temperature can be used to calculate the near-surface water vapor pressure, $P_{\text{H}_2\text{O}}$, at whichever height the TECP sensor was operating. We specifically used the portion of this data set that was collected “in-soil,” i.e., when the TECP probe’s needles were inserted into the soil. This was done to capture the temperature and water vapor abundance as close as possible to the planetary surface. Instead of using the temperature measured by the needles, we used the TECP board temperature as a proxy for soil temperature. This board temperature may be more accurate than that measured by the needles because the needle temperatures were likely cold-biased due to a lack of thermal conductivity with the regolith (Zent et al. 2010). The in-soil TECP data set included data from portions of 17 different sols between sols 46 and 150 of the 157 sol mission.

The air temperatures at 1.25, 1.5, and 2.0 m above the surface (0.25, 0.5, and 1.0 m above the lander deck) were measured by thermocouples on the mast of the Phoenix MET instrument. Here we use the air temperature furthest away from the surface, $T_{2\text{m}}$, for our analysis in order to limit thermal contamination due to the lander.

As in the case of the MSL analysis above, our deliquescence analysis at the Phoenix landing site focuses on the late evening and early morning hours because these are the only times that are potentially favorable for deliquescence. The measured TECP relative humidity near the surface was greater than or equal to 10% relative humidity only between 22:00 and 06:00 local time (Fischer et al. 2016). Near-surface conditions observed during this period were therefore used for our deliquescence analysis. Note that this is an 8 hr duration, the same as in the case of MSL, but it is offset by 1 hr. It can be seen in Figure 3 of Fischer et al. (2019) that overnight TECP data are primarily only available between sols 45 and 110 of the mission, with the 04:00–06:00 period the least densely covered by TECP measurements. Therefore, for all TECP in-soil data, we average over the range of sols from 45 to 110 and from 22:00 to 06:00.

During these time periods, the average derived $P_{\text{H}_2\text{O}}$ from the TECP instrument was 0.055 Pa (ranging from 0.015 to 0.204 Pa). This range of values is higher than the range of overnight $P_{\text{H}_2\text{O}}$ values from MSL REMS of 0.0064–0.085 Pa. The

average air temperature $T_{2\text{m}}$ was 197.7 K (ranging from 185.1 to 216.7 K). The average ground temperature, as approximated by the board temperature on the TECP RHS when the needles were in the soil, was 203.9 K (ranging from 188.4 to 231.1 K). The entire TECP ground temperature range overlapped with our experimental temperature range of 184–273 K, so no extrapolation of our uptake coefficient was required. To be consistent with the MSL analysis, we examine the same temperature range used above (175–235 K) in our Phoenix-relevant calculations.

Like for MSL, we used Equation (8) to determine the time required for complete deliquescence of a $\text{Ca}(\text{ClO}_4)_2$ particle at the Phoenix landing site assuming the water vapor flux resulting from the average near-surface atmospheric conditions present overnight when the relative humidity with respect to liquid was greater than 10% (from 22:00 to 06:00). We again assumed that the starting phase was $\text{Ca}(\text{ClO}_4)_2 \cdot 4\text{H}_2\text{O}$ and the final eutectic brine phase contained 50 wt% salt and 50 wt% water. This required that an additional 9.26 water molecules per formula unit be absorbed by the salt from the near-surface atmosphere. These deliquescence times are shown in Figure 8 as a function of particle size and ground temperature.

Figure 8 (Phoenix) appears very similar to Figure 7 (MSL). Larger particles and warmer temperatures result in longer deliquescence timescales, as expected. The horizontal gray lines denote different time periods ranging from 1 hr to 1 Martian yr. Conditions possibly conducive to deliquescence (average relative humidity > DRH) will only last a maximum of 8 hr sol^{-1} at the Phoenix landing site (22:00–06:00), so we will consider the size of a particle that could deliquesce in 8 hr. Given the ground temperature values measured during this time by TECP (188.4–231.1 K), particles with diameters ranging from 0.3 to 3 μm could potentially deliquesce during an 8 hr window. If only temperatures above the T_E are considered, then only particles less than 2 μm are likely to enter the aqueous phase. Metastable deliquescence may be able to occur, though, so the dashed lines should not be ignored. It should be noted that conditions at this location outside of this 104 sol period are not known. If a more complete seasonal record was measured at the Phoenix landing site, it would be possible to determine if there were environmental conditions that were even more conducive to brine formation.

One intriguing observation from the Phoenix mission involved images taken by the Robotic Arm Camera that appeared to show spheroids on a strut of the lander moving, growing, and merging over the course of several weeks. In addition to this liquid-like behavior, the spheroids may have also become darker and experienced growth proportional to volume, characteristics of a growing liquid phase. Renno et al. (2009) therefore suggested that these spheroids were liquid solutions, perhaps saline mud, that grew via salt deliquescence over this time period. These particles were on the order of 0.5–1.0 cm in diameter, and the growth appeared to be on the order of a few millimeters over several weeks, on average. Our experimental brine growth rates and timescales suggest that even a 1 mm $\text{Ca}(\text{ClO}_4)_2$ particle would require a full Martian year to fully deliquesce, assuming the conditions were favorable for deliquescence this entire time. Of course, in the actual Martian environment, the conditions may support brine formation for, at most, a third of the sol (the overnight hours), so complete deliquescence of a millimeter-scale particle does not seem feasible at the planetary surface. The shallow

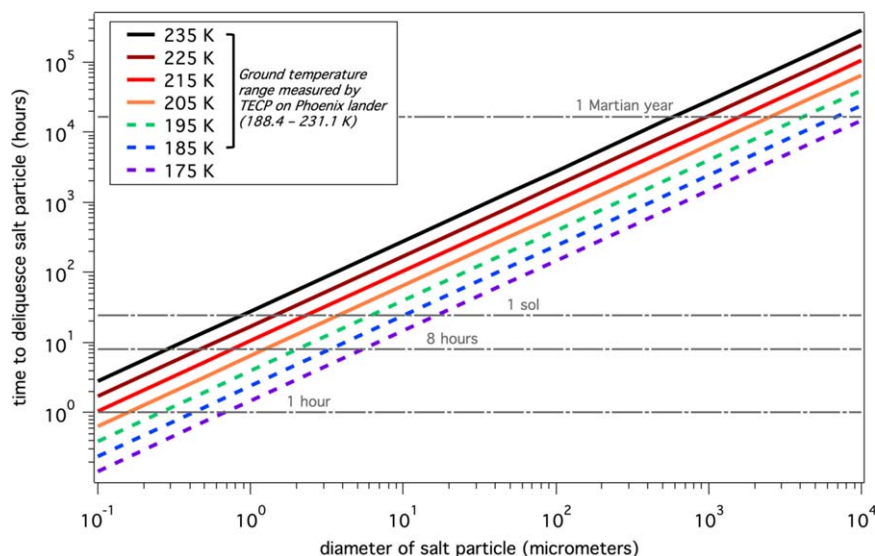


Figure 8. Time needed to fully deliquesce a $\text{Ca}(\text{ClO}_4)_2$ particle at the Phoenix landing site as a function of the salt particle diameter in microns and also the temperature of the salt particle. Solid colored lines are above the eutectic temperature of $\text{Ca}(\text{ClO}_4)_2$, and dashed colored lines are below the eutectic temperature (only metastable deliquescence possible). The higher water vapor pressures ($\sim 30\%$ higher) present at the Phoenix landing site compared to MSL result in shorter deliquescence timescales. Still, only particles $< 2 \mu\text{m}$ will be able to fully deliquesce in less than 8 hr if only temperatures above the eutectic temperature of $\text{Ca}(\text{ClO}_4)_2$ (198 or 199 K) are considered.

subsurface may produce slightly higher relative humidity conditions for extended periods (Nuding et al. 2014); thus, the subsurface environment may be more conducive to deliquescence. If the spheroids on the Phoenix lander strut did contain a brief or intermittent brine phase, this liquid may have been formed in the shallow subsurface from either deliquescence or the melting of ice in the salty regolith. It seems unlikely, though, that the full extent of the millimeter-scale growth reported by Renno et al. (2009) was due to atmospheric water uptake by deliquescent salts while the spheroids were on the lander strut.

The TECP instrument on the Phoenix lander was also able to investigate the potential formation of subsurface brine via electrical conductivity and dielectric permittivity measurements. Stillman et al. (2011) reported that measured changes in permittivity suggest that small amounts of liquid water may have been formed during certain times of day on certain sols. However, the lack of any detectable corresponding increase in electrical conductivity probably indicates that the brine phase is likely not continuous across the TECP needles; thus, the aqueous phase, if present, would only exist as “disconnected blobs or stringers” (Stillman & Grimm 2011). This is consistent with the brine growth rate results we report here. If only micron-scale salt grains can fully deliquesce at the Phoenix landing site (or micron-scale coatings develop on other salt grains), it is not expected that the spatial scale and distribution of these brines would ever reach pore space saturation or even continuous brine coatings across several millimeters. Of course, eutectic melting, brine forming from the melting of ice in contact with salt at temperatures at or above the T_E (not studied here), could still occur at the Phoenix landing site (Fischer et al. 2016).

5. Conclusion

Here we used a microscope outfitted with an environmental cell to experimentally investigate the growth rate of Mars-relevant calcium perchlorate brines. Studies were performed

over a range of temperatures (184–273 K) and water vapor pressures (0.2–220 Pa), the main factors that impact water uptake kinetics. By comparing the observed growth to the theoretical growth if $\gamma = 1$, we determined a temperature-dependent net uptake coefficient for gas phase water molecules colliding with a perchlorate brine surface. The average values of this net uptake coefficient ranged from 3.8×10^{-4} at 185 K to 4.2×10^{-6} at 273 K. These net values captured the balance of water uptake and loss during the time period between consecutive microscope measurements, 3–15 minutes apart.

These values of the temperature-dependent net uptake coefficient were used to estimate deliquescence rates at two locations on Mars where the near-surface environmental conditions have been measured: along the Curiosity rover traverse at equatorial Gale Crater and the northern midlatitude Phoenix landing site. Although we have experimentally measured the growth rate of an already-deliquesced brine particle, the uptake coefficient was used to estimate the time needed for a given size particle to fully deliquesce on Mars. Once deliquescence was initiated, the process would still require uptake of water molecules by a brine surface; thus, our experimental $\gamma_{\text{net}}(T)$ values (the net uptake of water vapor molecules onto a brine surface) are still relevant to deliquescence on Mars.

At both the Gale Crater and Phoenix landing site locations, ground temperature and near-surface relative humidity conditions are only possibly conducive to deliquescence overnight and for at most 8 hr sol^{-1} . We determined that water uptake by calcium perchlorate at either of these locations is fairly slow. In 8 hr, only salt grains that are $2 \mu\text{m}$ or smaller (or salt coatings $2 \mu\text{m}$ or thinner) would have time to completely deliquesce when temperatures are above T_E . Deliquescence rates at the Phoenix landing site are approximately 30% faster than at Gale Crater, with the difference primarily due to the higher water vapor pressures present at the higher latitudes of Phoenix. These results do not rule out deliquescence or brine growth occurring but suggest that any brine formed through this

process is present on a very small scale that may not be detectable using conductivity or imaging techniques.

These results help interpret the variation in experimental results in the literature, with some studies finding that deliquescence occurs almost immediately when conditions are favorable (Zorzano et al. 2009; Gough et al. 2011; Nuding et al. 2014), while others report that deliquescence is too slow to be relevant to Mars (Fischer et al. 2014). The discrepancy is likely to be due to differences in the grain size of the salt sample and the water partial pressure present during experiments. The uptake coefficient values we measure here could be applied to any system where salt and water vapor are present, deliquescence may occur, and a timescale of brine growth is desired.

We are grateful to Dr. Cecilia Leung for the Phoenix TECP “in-soil” data set and Dr. Shuichi Ushijima for assistance with the LabVIEW particle sizing program that he created. R.V.G. and M.A.T. acknowledge the MSL PSP program for funding. E.G.R.V. acknowledges support from NASA through the Habitable Worlds program under grant No. 80NSSC17K0742.

The Phoenix TECP data are available on the PDS at <https://pds-geosciences.wustl.edu/missions/phoenix/martinez.htm>. The MSL REMS data are available on the PDS at https://atmos.nmsu.edu/data_and_services/atmospheres_data/MARS/curiosity/rem.html. The data behind the figures in this paper, as well as all experimental data, can be downloaded at https://scholar.colorado.edu/concern/data_sets/st74cr92w. Publication was funded by the University of Colorado Boulder Libraries Open Access Fund.

ORCID iDs

Raina V. Gough  <https://orcid.org/0000-0003-2755-7282>
Edgard G. Rivera-Valentín  <https://orcid.org/0000-0002-4042-003X>

References

- Baustian, K. J., Wise, M. E., & Tolbert, M. A. 2010, *ACP*, **10**, 2307
 Catling, D. C., Claire, M. W., Zahnle, K. J., et al. 2010, *JGRE*, **115**, E00E11
 Chevrier, V. F., Hanley, J., & Altheide, T. S. 2009, *GeoRL*, **36**, L10202
 Chevrier, V. F., Rivera-Valentín, E. G., Soto, A., & Altheide, T. S. 2020, *PSJ*, **1**, 64
 Clark, J., Sutter, B., Archer, P. D., et al. 2021, *Mine*, **11**, 475
 Davidovits, P., Worsnop, D. R., Jayne, J. T., et al. 2004, *GeoRL*, **31**, L22111
 Fischer, E., Martinez, G. M., Elliott, H. M., & Renno, N. O. 2014, *GeoRL*, **41**, 4456
 Fischer, E., Martinez, G. M., & Renno, N. O. 2016, *AsBio*, **16**, 937
 Fischer, E., Martinez, G. M., Renno, N. O., Tamppari, L. K., & Zent, A. P. 2019, *JGR*, **124**, 2780
 Fung, K. H., Tang, I. N., & Munkelwitz, H. R. 1987, *ApOpt*, **26**, 1282
 Glavin, D. P., Freissinet, C., Miller, K. E., et al. 2013, *JGR*, **118**, 1955
 Gough, R. V., Chevrier, V. F., Baustian, K. J., Wise, M. E., & Tolbert, M. A. 2011, *E&PSL*, **312**, 371
 Gough, R. V., Nuding, D. L., Archer, P. D., et al. 2020, *GeoRL*, **47**, 12180
 Gough, R. V., Primm, K. M., Rivera-Valentín, E. G., Martinez, G. M., & Tolbert, M. A. 2019, *Icar*, **321**, 1
 Harri, A.-M., Genzer, M., Kemppinen, O., et al. 2014, *JGRE*, **119**, 2132
 Haynes, D. R., Tro, N. J., & George, S. M. 1992, *JPhCh*, **96**, 8502
 Hecht, M. H., Kounaves, S. P., Quinn, R. C., et al. 2009, *Sci*, **325**, 64
 Heinz, J., Schulze-Makuch, D., & Kounaves, S. P. 2016, *GeoRL*, **43**, 4880
 Kounaves, S. P., Chaniotakis, N. A., Chevrier, V. F., et al. 2014, *Icar*, **232**, 226
 Marion, G. M., Catling, D. C., Zahnle, K. J., & Claire, M. W. 2010, *Icar*, **207**, 675
 Martinez, G. M., Fischer, E., Renno, N. O., et al. 2016, *Icar*, **280**, 93
 Martinez, G. M., Newman, C. N., De Vicente-Retortillo, A., et al. 2017, *SSRv*, **212**, 295
 Martinez, G. M., Vicente-Retortillo, A., Vasavada, A. R., et al. 2021, *JGRE*, **126**, e06804
 Martín-Torres, F. J., Zorzano, M., Valentín-Serrano, P., et al. 2015, *NatGeo*, **8**, 357
 Nikolakakos, G., & Whiteway, J. A. 2015, *GeoRL*, **42**, 7899
 Nuding, D. L., Gough, R. V., Venkateswaran, K. J., Spry, J. A., & Tolbert, M. A. 2017, *AsBio*, **17**, 997
 Nuding, D. L., Rivera-Valentín, E. G., Davis, R. D., et al. 2014, *Icar*, **243**, 420
 Pal, B., & Kereszturi, A. 2017, *Icar*, **282**, 84
 Pál, B. D., & Kereszturi, Á. 2022, *Icar*, **376**, 114856
 Peng, C., Chen, L., & Tang, M. 2021, *Fundamental Research*, **2**, 578
 Pestova, O. N., Myund, L. A., Khripun, M. K., & Prigaro, A. V. 2005, *J. Appl. Chem.*, **78**, 409
 Primm, K. M., Gough, R. V., Chevrier, V. F., & Tolbert, M. A. 2017, *GeCoA*, **212**, 211
 Renno, N. O., Bos, B. J., Catling, D., et al. 2009, *JGRE*, **114**, E00E03
 Rivera-Valentín, E., Martinez, G., Filiberto, J., et al. 2021, *BAAS*, **53**, 091
 Rivera-Valentín, E. G., Chevrier, V. F., Soto, A., & Martinez, G. 2020, *NatAs*, **4**, 756
 Rivera-Valentín, E. G., Gough, R. V., Chevrier, V. F., et al. 2018, *JGRE*, **123**, 1156
 Sebastián, E., Armiens, C., Gómez-Elvira, J., et al. 2010, *Sensors*, **10**, 9211
 Stern, J. C., Sutter, B., Jackson, W. A., et al. 2017, *GeoRL*, **44**, 2643
 Stillman, D. E., & Grimm, R. E. 2011, *JGR*, **116**, E09005
 Tamppari, L. K., Martínez, G., Rodríguez-Manfredi, J. A., et al. 2022, in Seventh International Workshop on the Mars Atmosphere: Modelling and Observations (Paris), https://hal-insu.archives-ouvertes.fr/insu-03750951/file/oral_Tamppari_Leslie.pdf
 Tang, M. J., & Shiraiwa, M. 2015, *ACP*, **15**, 5585
 Taylor, P. A., Catling, D. C., Daly, M., et al. 2008, *JGRE*, **113**, E00A10
 Toner, J. D., Catling, D. C., & Light, B. 2014, *Icar*, **233**, 36
 Wang, A., Ling, Z., Yan, Y., et al. 2019, *Icar*, **333**, 464
 Zent, A. P., Hecht, M. H., Cobos, D. R., et al. 2010, *JGRE*, **115**, E00E14
 Zorzano, M. P., Mateo-Martí, E., Prieto-Ballesteros, O., Osuna, S., & Renno, N. 2009, *GeoRL*, **36**, L20201